38th International Electric Vehicle Symposium and Exhibition (EVS38) Göteborg, Sweden, June 15-18, 2025

Beyond Full Charge: Battery storage technology agnostic Real-Time SoH Estimation Using AI and Genetic Algorithms

M. Azkue[1], J. Olmos[1], M. Usabiaga[1], I. Gandiaga[1]

[1] *Ikerlan Technology Research Centre, Basque Research and Technology Alliance (BRTA). P° J.M. Arizmendiarrieta, 2, 20500 Arrasate-Mondragón, Spain, mazkue@ikerlan.es*

Executive Summary

This work tackles state of health (SoH) estimation for NMC Li-ion, essential for enhancing safety and efficiency of the batteries in various applications. Using neural networks and the partial charge method, an estimation algorithm has been designed to calculate the SoH without the need to perform a full charge of the battery. The methodology includes the use of the NSGA-II optimisation algorithm, which allows defining optimal voltage ranges to increase the accuracy and applicability of the estimator in real conditions. Preliminary results with NMC cells show that the model is robust and reliable in estimating the SoH. Finally, Transfer Learning will be used to analyse the adaptability, robustness and reliability of the developed algorithm for Na-ion batteries.

Keywords: Electric vehicles, Battery Management System, Energy Storage Systems, Energy management, AI – Artificial intelligence for EVs

1 Introduction

Over the past few decades, lithium-ion batteries (LIBs) have established their role as one of the most efficient and versatile energy storage technologies. Their high energy density, long life, low self-discharge rate and predictable behaviour have made them suitable for a wide range of applications, from portable electronics to electric vehicles (EVs) and stationary storage systems. Although their commercialization began in 1991 with Sony, the real boom has come in recent years, driven by the need to reduce greenhouse gas emissions and adopt more sustainable energy solutions [1].

The electric mobility sector has been one of the main drivers of this evolution. From the first electric vehicles such as the Nissan Altra, with a range limited to around 190 km, to today's models that exceed 700 km, progress has been remarkable. However, the key objectives remain the same: increase energy density, reduce weight, extend system life, maintain safety and reduce associated costs. All this must be achieved in a highly variable operating environment, where batteries are subject to multiple charge and discharge cycles, temperature fluctuations and different usage profiles.

In this context, the Battery Management System (BMS) plays a central role. This system not only ensures that the battery operates within the safe limits defined by the Safe Operating Area (SOA) but also takes care of critical tasks such as cell balancing, data collection, fault detection and, especially, the estimation of internal states that cannot be measured directly. One of these states is the State of Health (SoH), which represents a key metric for assessing battery degradation, determining its remaining functional capacity and planning preventive maintenance or replacement tasks [2].

SoH can be defined in several ways, the most common being the residual capacity with respect to the initial nominal value, or the increase in the cell's internal resistance over time. However, its precise estimation is challenging, as it depends on numerous factors such as temperature, charge/discharge profile, depth of discharge (DoD) or number of cycles. Furthermore, degradation of LIBs occurs both by calendar aging - even at rest - and by cycling aging, derived from the charge and discharge processes [3,4].

In order to address this challenge, several SoH estimation methods have been developed. These can be classified into four main groups: direct measurements, indirect measurements, models based on physicochemical equations, and data-driven models. Direct and indirect methods are useful in controlled laboratory environments but are impractical in real applications due to their complexity, cost or dependence on specific operating conditions. Methods based on physical-mathematical models allow in situ estimations with high accuracy, but require a detailed characterization of the cell, a thorough knowledge of its chemistry and internal processes, as well as considerable computational effort. Moreover, their applicability to different cell types is limited, as each variant requires a specific adaptation of the model [5–9].

In the face of these limitations, data-driven models have gained prominence due to their generalizability, robustness to noisy data and flexibility. These models do not require prior characterization of the cell or detailed knowledge of its internal reactions, which makes them easily applicable to different types of batteries and configurations. Their main drawback lies in the need for large volumes of representative data to achieve adequate training, as well as the computational effort required during the development phase. However, the growth in the number of systems equipped with advanced BMSs - capable of recording multiple operating variables and generating historical databases - has facilitated access to these data, making the application of data-driven models in real environments feasible and increasingly cost-effective[10–12].

Within this category, two major subgroups can be distinguished: traditional Machine Learning models and models based on neural networks (NN). Although both approaches offer interesting advantages, this paper opts for the use of neural networks due to their greater capacity to model complex nonlinear relationships, as well as their compatibility with advanced techniques such as Transfer Learning (TL). This technique allows reusing previously trained models in a given domain and adapting them to new data sets with different characteristics, thus avoiding the training of a new NN from scratch. In the case of LIBs, TL enables knowledge transfer between cells with different capacities, configurations, or even different chemical compositions, such as sodium batteries. This significantly extends the scope and practical utility of the developed models, further consolidating the choice of neural networks as the basis of the proposed estimator [8,13–16].

This paper presents a neural network-based methodology for SoH estimation of NMC lithium-ion batteries. The paper is organized as follows: Section 2 describes the proposed SoH estimator, detailing the model architecture and the training methodology followed. Section 3 presents the case studies developed, together with the results obtained and their analysis. Finally, Section 4 presents the conclusions of the work and possible future lines of research.

2 SoH estimation algorithm

2.1 Dataset overview

The estimator developed in this project has been trained using experimental data obtained from lithium-ion pouch cells with a nominal capacity of 58 Ah, based on NMC/graphite chemistry. To generate the dataset, the cells were subjected to a wide range of operating conditions with the aim of capturing diverse degradation patterns and behaviours. This diversity is key to ensuring that the estimator is robust and capable of generalizing well to unseen conditions.

High-quality data is essential for building a reliable NN model. Accurate, diverse, and representative data allow the model to effectively learn the underlying degradation dynamics and produce precise SoH estimations. To this end, the cells were cycled under various controlled conditions, including different ambient temperatures, charge/discharge current rates, DoD, and average state-of-charge (SoC) levels. These parameters were chosen to simulate a broad range of realistic usage scenarios.

Data collection

Generating a degradation dataset is inherently time-consuming due to the slow nature of battery aging, which progresses over hundreds or even thousands of charge-discharge cycles. Each cell in the dataset was subjected to specific cycling conditions, as summarized in Table 1, encompassing a diverse set of stress profiles to provide a rich training base for the model.

Table 1 includes the following columns: the Cell identifier; the Charge C-rate and Discharge C-rate used during cycling; the DoD percentage; the Mid. SoC around which the cycling was centered; the temperature at which the tests were conducted; the dataset split designation (Training, Validation, or Test) indicating how the cell data was used during model development; and finally, the color corresponding to each cell as shown in the Figure 1 for easier visual reference.

Table 1. Cells cycling condition matrix.

Cell	CHA C-rate	DCH C-rate	DoD	Mid. SoC	Temperature	Used for	Color
C01	1C	C/3	70 %	45 %	25 °C	Train/Validation	
C02	2C	C/3	70 %	45 %	25 °C	Train/Validation	
C03	C/3	1C	100 %	50 %	25 °C	Train/Validation	
C04	C/3	1C	20 %	20 %	25 °C	Train/Validation	
C05	C/3	1C	20 %	50 %	25 °C	Test	
C06	C/3	1C	20 %	80 %	25 °C	Train/Validation	
C07	C/3	1C	50 %	50 %	25 °C	Test	
C08	C/3	1C	70 %	45 %	25 °C	Train/Validation	
C09	C/3	1C	80 %	50 %	25 °C	Train/Validation	
C10	C/3	1C	80 %	50 %	45 °C	Test	
C11	C/3	C/3	70 %	45 %	25 °C	Train/Validation	
C12	C/3	C/3	80 %	50 %	45 °C	Train/Validation	

To accurately track the SoH of each cell, periodic reference tests known as Check-Ups (CUs) were performed. These tests involved three consecutive full charge and discharge cycles under standardized conditions—constant current (0.5C) at 25°C—repeated every 100 Full Equivalent Cycles (FEC). From each CU, the SoH was calculated using the final two discharge cycles and the following equation:

$$SoH = \frac{Ah_{Dch}\ at\ cycle\ n}{Ah_{Dch}\ at\ cycle\ 0} \quad (1)$$

This approach provided a reference SoH curve for each cell, allowing the quantification of degradation over time. As shown in Figure 1, cell C02 exhibited the most pronounced degradation, reaching a SoH of 64.34% after 832 FEC, mainly due to a high charge current of 2C. Cells C10 and C12 also showed significant aging, ending around 90% SoH after over 900 FEC, which is attributed to their operation at elevated temperatures (45°C). In contrast, cells such as C04 maintained a SoH above 94.47% even after more than 1500 FEC, indicating a slower degradation under milder cycling conditions.

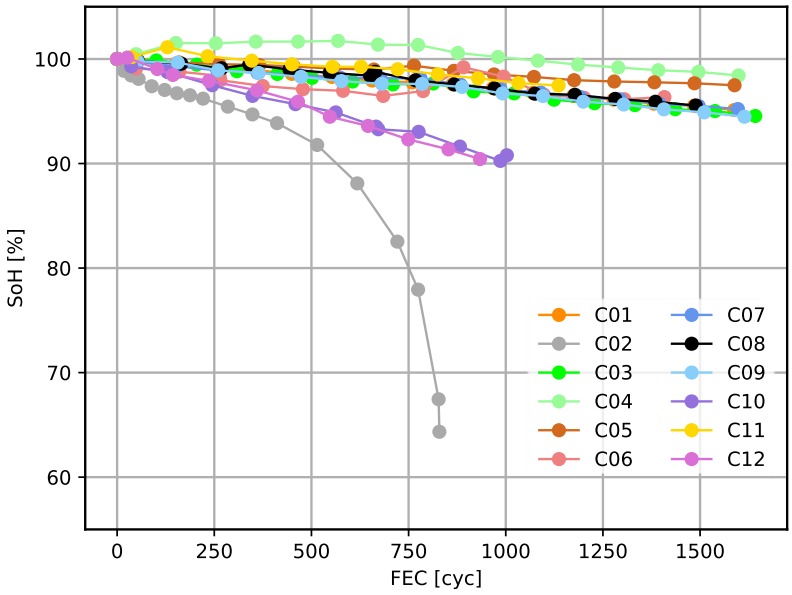

Figure 1. SoH degradation curves

This variability in degradation was a key factor in the partitioning of the dataset into training, validation, and test sets. Since NN models typically perform best when evaluated on data distributions similar to

those seen during training, the most and least degraded cells (C02 and C04) were included in the training and validation sets to span the full degradation range. Similarly, from the two high-temperature cells (C10 and C12), one was used for training/validation and the other for testing. Cell C07 was selected to represent a cluster of cells with similar behaviour, and cell C05 was added to the test set as an intermediate degradation case. This careful selection strategy ensures a balanced dataset that enhances model generalization and robustness.

Partial charge method

In real-world applications, it is rare to perform full charge or discharge cycles—especially with constant current-constant voltage (CC-CV) protocols—as most battery systems operate within partial state-of-charge windows. To reflect this reality and develop a practical SoH estimator, the approach adopted in this work relies on the analysis of partial charge segments.

Three distinct voltage windows were defined for this purpose: 3.6–3.8 V, 4.0–4.2 V, and 3.5–4.25 V. These segments allow the estimator to assess battery health without requiring complete cycles, thus mimicking typical usage conditions in electric vehicles and energy storage systems.

To estimate the SoH using these partial charges, a modified version of the original SoH formula was used. Instead of relying on discharged capacity, the SoH is computed using the charged capacity within each voltage window:

$$SoH_{V_{window}} = \frac{Ah_{Cha}\ at\ cycle\ n}{Ah_{Cha}\ at\ cycle\ 0} \quad (2)$$

This adjustment is justified by the fact that charge profiles are generally more consistent and controllable across applications, while discharge profiles vary significantly depending on the system's energy demands.

In addition, an optimization algorithm has been integrated into the methodology to identify the most informative voltage windows. This algorithm systematically selects the ranges that provide the best correlation between partial charge capacity and overall SoH, thereby improving the performance of the final estimator. A detailed description of the optimization process is provided in the following section.

2.2 Optimization algorithm: NSGA-II

The selection of appropriate voltage windows is a key factor in the development of a robust SoH estimator. These windows must strike a balance between being wide enough to capture meaningful information and narrow enough to be realistically applicable in real-world use cases. Wider voltage windows tend to yield more accurate estimations, but they are less likely to occur during typical battery operation, limiting their practical utility.

To identify optimal voltage windows, several optimization strategies were considered. Single-objective methods such as grid search were discarded in favour of multi-objective approaches, given the bi-objective nature of the problem. To achieve the best trade-off between estimation accuracy and voltage window size, the Non-dominated Sorting Genetic Algorithm II (NSGA-II) was selected. NSGA-II is a genetic algorithm designed for multi-objective optimization, capable of finding a diverse set of optimal solutions—known as the Pareto front—without requiring explicit weighting of the objectives [17].

The first step in implementing the optimization algorithm was to define the two objective functions to minimize. The first objective, shown in equation (3), represents the absolute error between the actual SoH value (SoH_{real}) and the value estimated from a given voltage window (SoH_{window}). The second objective, shown in equation (4), corresponds to the amplitude of the voltage window, where V_1 and V_2 define the lower and upper voltage limits, respectively:

$$f_1 = |SoH_{real} - SoH_{window}| \quad (3)$$

$$f_2 = V_2 - V_1 \quad (4)$$

Both objectives are minimized to achieve high estimation accuracy while maintaining a narrow voltage range.

NSGA-II begins with an initial population of candidate solutions, where each individual (chromosome) is defined by a pair of voltage values ($V1, V2$), representing the boundaries of a potential charge window. A full population consists of many such chromosomes, and its size is a hyperparameter that must be carefully tuned to ensure a good balance between exploration, accuracy, and computational cost.

For each chromosome, the algorithm performs the following steps: (1) all partial charge segments within the defined voltage window are extracted from the dataset; (2) the charged capacity in this range is computed; (3) the SoH is calculated using equation (12); and (4) the fitness values f_1 and f_2 are evaluated. Once all individuals are evaluated, the population is ranked using non-dominated sorting to classify solutions into Pareto fronts—sets of non-dominated solutions where no objective can be improved without degrading the other [12,18].

To preserve diversity in the solution space, a crowding distance metric is assigned to each individual within a Pareto front. This metric ensures that the algorithm favours both optimality and solution spread by prioritizing individuals located in less crowded regions of the front [11,19].

The next generation is formed by combining the current population P_t and its offspring Q_t, creating a union R_t. This set is sorted into Pareto fronts, and the best N individuals are selected to form the next population P_{t+1}, as illustrated in Figure 2. If more individuals are needed to complete the new population, those with the highest crowding distance within the last selected front are chosen.

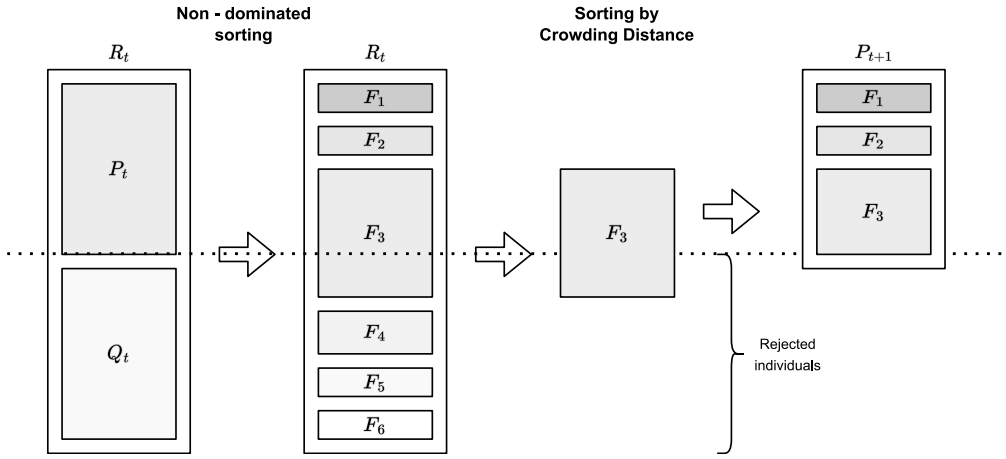

Figure 2. Procedure of NSGA-II algorithm.

The process of the full optimization procedure begins with the dataset selection and initialization of a random population. Chromosomes are evaluated using the defined objectives, and genetic operations such as crossover and mutation are applied. The new solutions are merged with the existing population, sorted, and the best ones are selected to continue. This loop continues until either a stopping criterion is met—specifically, a mean error below 0.25% and a voltage window narrower than 200 mV—or the maximum number of iterations is reached.

An example result of this optimization process is presented in Figure 3, which shows the Pareto front obtained for cell C10. The x-axis represents the voltage range width, while the y-axis shows the average error in SoH estimation using the partial charge method. As expected, wider voltage windows result in lower errors, though they are harder to achieve in practical applications due to typical charging limitations.

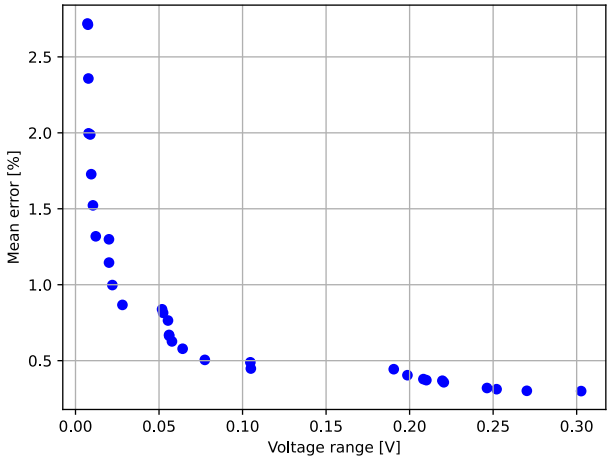

Figure 3. Pareto front of cell C10.

After optimizing the voltage windows for all cells, a post-analysis was carried out to evaluate their estimation capabilities. While the estimations did not fully match the actual SoH values, particularly in

the case of narrow voltage windows, some degradation patterns were still captured. In the case of cell C07, the estimated SoH curve resembled the trend of the actual curve, suggesting that voltage window information, although not sufficient on its own, contains useful features. Therefore, rather than using voltage windows as a standalone estimation method, they are incorporated as one of the input features in the neural network models described in the following section.

3 Case studies

In this section, the different case studies developed during the project are presented. Each case study involves the training of a specific NN model with a particular set of input features. The training process, evaluation methodology, and obtained results are discussed in detail for each case, with the aim of identifying which configurations are most suitable for accurate SoH estimation using partial charge data.

The dataset employed was generated from laboratory measurements obtained by cycling the cells under the conditions specified in Table 1. A total of 25% of the available data—corresponding to three cells—was reserved exclusively for testing purposes. The remaining 75% was randomly split into training (80%) and validation (20%) subsets.

In terms of data preprocessing, only standardization was applied, aiming to normalize the feature scales and facilitate the NN training process. This step mitigates the risk of feature dominance due to varying magnitudes and contributes to improved convergence during training. No outlier removal or additional filtering was applied, in order to preserve the dataset's integrity and retain all potentially relevant information.

Model optimization was carried out via hyperparameter sweeps platform, which enables real-time monitoring of the training process and performance metrics, as well as detailed visualization of results.

3.1 Model 1

The first model developed in this study consists of five input features and a single output corresponding to the estimated SoH. The selected inputs are:

- V_1: the initial voltage value of the window used.
- dV: dimension of the voltage window used.
- $\mathrm{AhCha}_{\mathrm{window}}$: ampere-hours charged in the voltage window used.
- $\mathrm{C\text{-}rate}_{\mathrm{window}}$: average C-rate in the voltage window used.
- $\mathrm{Temperature}_{\mathrm{window}}$: average temperature in the voltage window used.

The aim of this model is to assess whether the SoH can be reliably estimated using only information related to a limited voltage range, in addition to the corresponding charged capacity and environmental conditions. A hyperparameter sweep was conducted using W&B to identify the most suitable model configuration. The resulting sweep and corresponding error metrics, including Maximum Error and MAE, are presented in Figure 4.

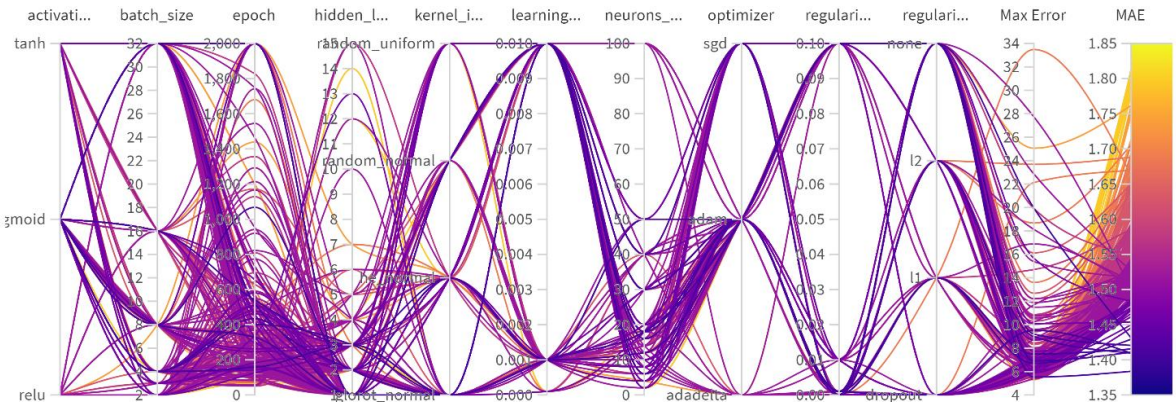

Figure 4. Hyperparameter sweep of Model 1.

The test results for Model 1 are illustrated in Figure 5, which presents the SoH estimations and corresponding percentage errors for three different cells. The estimation was performed using a voltage window of 0.13 V, specifically from 3.74 V to 3.87 V.

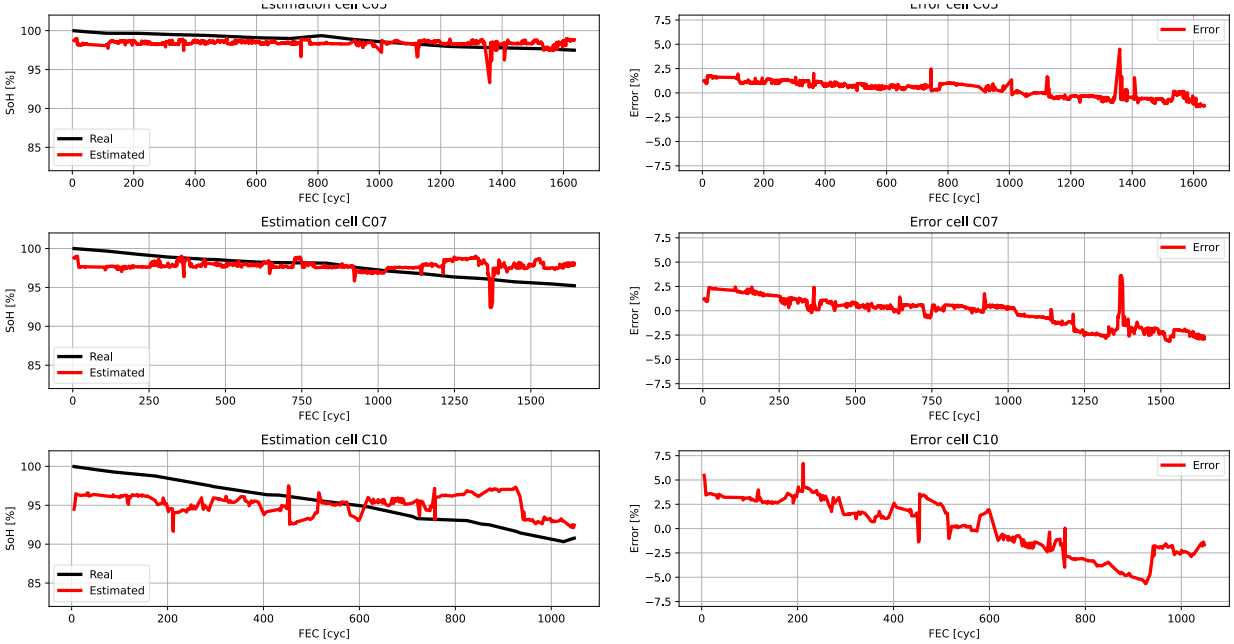

Figure 5. SoH estimations and errors of the Model 1 using a voltage range of 0.13 V (from 3.74 V to 3.87 V).

The results clearly indicate the model's limited ability to track the actual degradation trends. For instance, in cell C05, estimations remain nearly constant around 98.5% across most cycles, except for a sharp drop between FEC 1340 and 1365, coinciding with a significant increase in temperature (up to 45°C). A similar temperature-induced effect is observed in cell C07 between cycles 1360 and 1365. However, an anomalous overestimation is seen from cycle 1200 onward, which is not reflected in the actual SoH evolution. As for cell C10, the model fails to follow the degradation trend at any point. Moreover, the model does not correctly identify the BoL stage, as none of the test cells start with SoH estimations near 100%.

The quantitative metrics obtained during training, validation, and testing phases are summarized in Table 2:

Table 2. SoH estimation errors for Model 1.

	Max. Error	**MAE**
Train	16.79%	0.84%
Validation	12.05%	0.85%
Test	7.68%	1.38%

These results confirm that, although the model can achieve low average errors in the training and validation sets, it lacks the ability to generalize well or to reflect realistic SoH dynamics on unseen data. The relatively poor performance, particularly on the test cells, suggests that using only partial charge and environmental data within a constrained voltage range is insufficient for accurate SoH estimation.

Model 2A

After analysing the results obtained with Model 1, it was decided to incorporate an additional input to the model. The goal of this modification is to enable the neural network to learn that the SoH typically decreases over time and usage. To this end, two different models were trained and compared: in the first one, a column named dT was added; in the second one, a column named FEC was included. dT represents the elapsed time from the BoL to the current point, while FEC indicates the total number of full charge/discharge cycles the cell has undergone since BoL.

As previously mentioned, Model 2A includes the five input variables from Model 1 — V_1, dV, $\text{AhCha}_{\text{window}}$, $\text{C-rate}_{\text{window}}$, $\text{Temperature}_{\text{window}}$ — plus the new time-related input 'dT'. A new hyperparameter sweep was conducted. Using the hyperparameters that obtained the best results during the sweep, Model 2A was trained and tested. The results are presented in Figure 6.

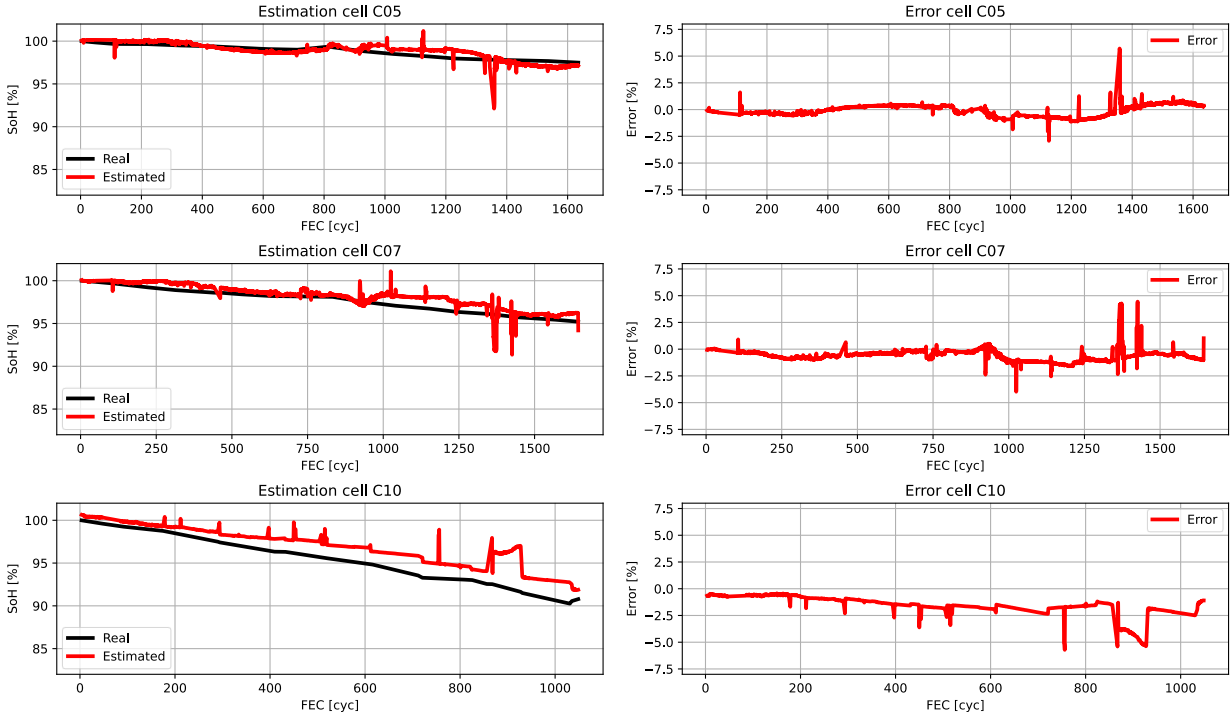

Figure 6. SoH estimations and errors of Model 2A using a voltage range of 0.13 V (from 3.74 V to 3.87 V).

The inclusion of the dT variable significantly improved model performance compared to Model 1. Notably, SoH estimations now begin near 100%, consistent with expected BoL values. However, for cell C10, the model still fails to capture the actual degradation trajectory.

In cell C05, significant discrepancies appear between 1340 and 1365 FEC, correlated with a temperature increase from 28°C to 45°C. A similar pattern emerges in cell C07 between 1360 and 1425 FEC, where the temperature rises to 41.5°C. In cell C10, the model also exhibits an unrealistic SoH increase from 94% at cycle 857 to 97% at cycle 931.

Despite some errors, the MAE on test data improved compared to Model 1. The full metrics are listed in Table 3.

Table 3. SoH estimation errors for Model 2a.

	Max. Error	MAE
Train	20.34%	0.67%
Validation	13.86%	0.71%
Test	6.71%	0.77%

Model 2B

Model 2B was developed to compare the effect of using FEC instead of dT as the temporal variable. All other input variables remain the same. A hyperparameter sweep was again performed. Model 2B was trained then with the best hyperparameters identified through the sweep. The results are shown in Figure 7.

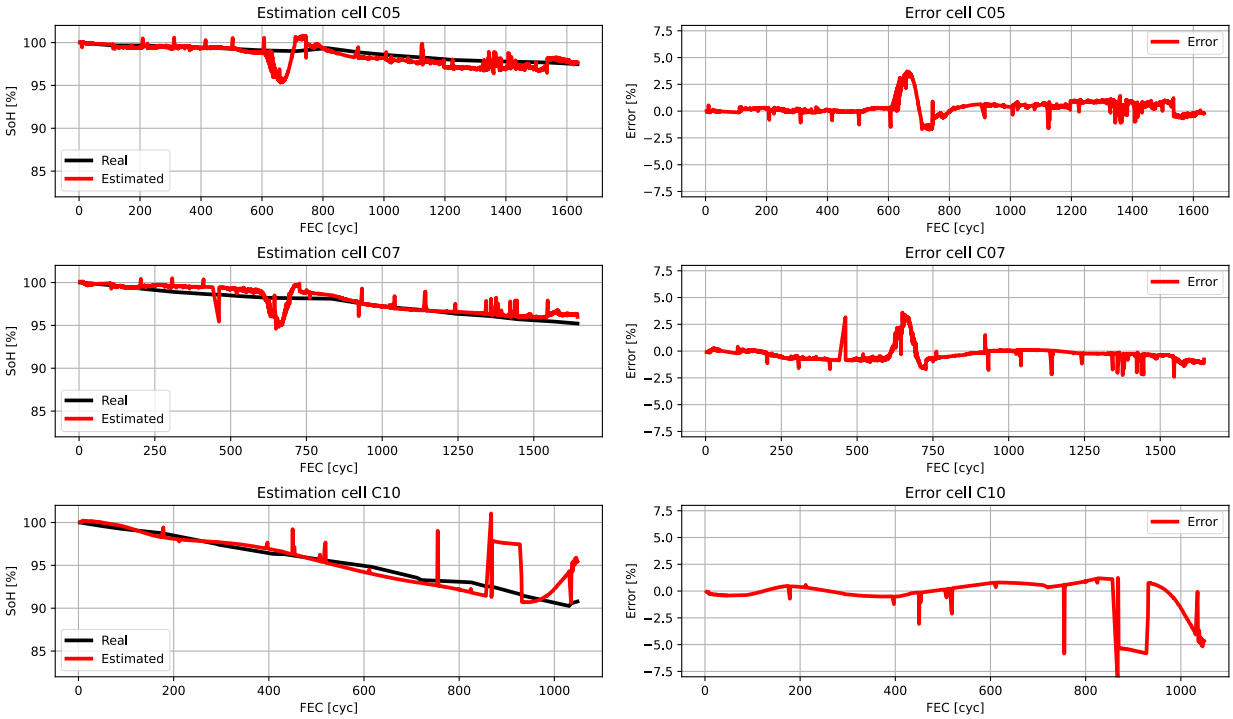

Figure 7. SoH estimations and errors of Model 2B using a voltage range of 0.13 V (from 3.74 V to 3.87 V).

As in Model 2A, the inclusion of a temporal variable allowed the SoH estimations to start at values close to 100%. Moreover, Model 2B demonstrates superior performance in capturing the overall degradation trend. For instance, as shown in Figure 7, unlike Model 2A, Model 2B closely tracks the real SoH curve over time. However, deviations still appear — for example, in cells C05 and C07 between 600 and 800 FEC — possibly due to overfitting [20].

In cell C10, SoH estimations increase from 92% to 98% between 830 FEC and subsequent cycles, which coincided with a temperature drop from ~45°C to ~29°C. This indicates the NN may be incorrectly correlating current temperature with SoH. In practice, SoH should not fluctuate with ambient conditions like daily temperature variation, highlighting a critical modelling flaw. It is important to note that SoH is a long-term indicator of battery health, and short-term temperature changes should not cause variations in SoH estimations unless the changes are extremely severe.

To address this, Model 3 was developed with new features that aim to decouple transient effects like current temperature from long-term degradation indicators. The performance metrics for Model 2B are presented in Table 4, demonstrating consistent improvements across all phases when compared to Model 2A.

Table 4. SoH estimation errors for Model 2B.

	Max. Error	MAE
Train	6.53%	0.40%
Validation	6.17%	0.43%
Test	6.09%	0.56%

Model 3

As previously discussed, Models 2A and 2B exhibited an undesired correlation between the instantaneous temperature and the predicted SoH values, leading to unrealistic estimations that weaken model reliability. To address this issue, Model 3 introduces seven new features—four related to C-rate and three to the temperature—designed to provide the model with cumulative historical context rather than instantaneous values.

The new input variables are detailed below and are a percentage of time the cell operated in certain conditions since BOL:

- C-rate_0: Percentage of time the cell operated with zero current (C = 0).
- C-rate_1: Percentage of time the cell operated within the range $-1 \leq C < 0$ or $0 < C \leq 1$.
- C-rate_1-2: Percentage of time the cell operated within $-2 \leq C < -1$ or $1 < C \leq 2$.

- C-rate_2: Percentage of time the cell operated with C < −2 or C > 2.
- Temperature_10: Percentage of time the cell experienced a temperature ≤ 10 ℃.
- Temperature_10–35: Percentage of time the cell operated within 10 ℃ < T ≤ 35 ℃.
- Temperature_35: Percentage of time the cell experienced a temperature > 35 ℃.

These variables allow the model to learn the impact of thermal and electrical stress on degradation over the cell's lifetime, minimizing the influence of momentary fluctuations in operating conditions. A hyperparameter sweep was conducted again to fine-tune the model for optimal performance.

Using the best hyperparameters, Model 3 was trained, and the resulting SoH estimations are shown in Figure 8.

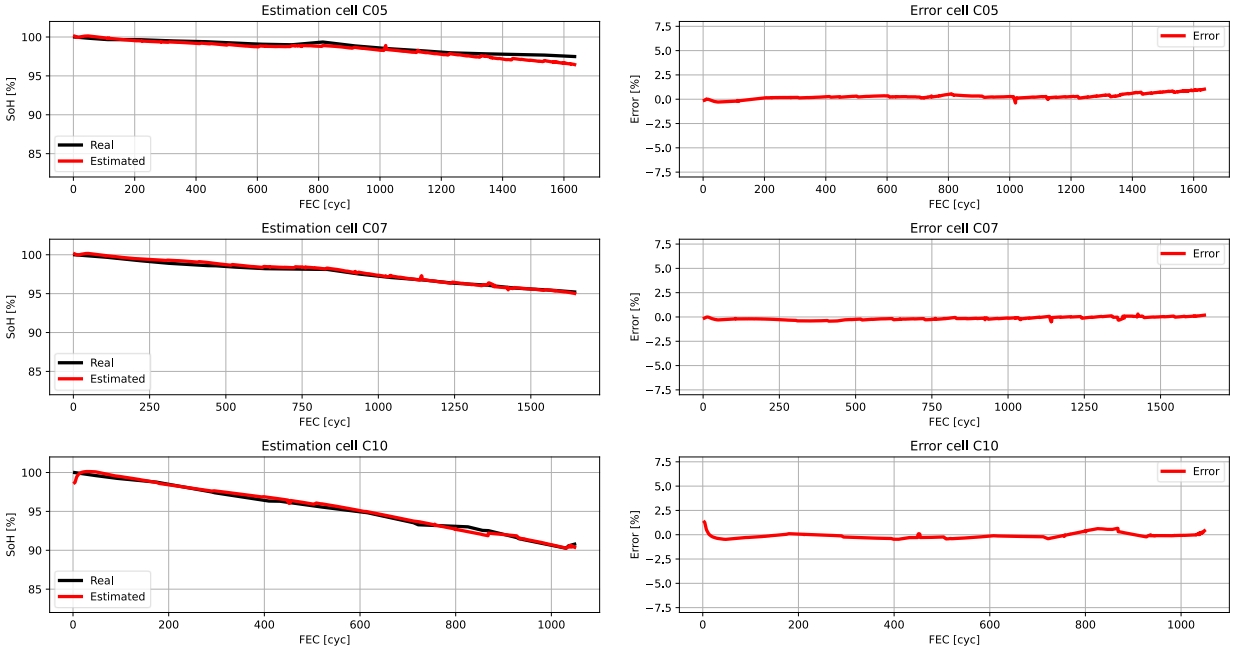

Figure 8. SoH estimations and errors of the Model 3 using a voltage range of 0.13 V (from 3.74 V to 3.87 V).

The estimations reveal a substantial improvement in stability and accuracy. Notably, abrupt SoH fluctuations present in previous models have been successfully mitigated. For cell C05, the predictions are accurate, with only slight deviation observed beyond 1300 FEC. Cell C07 displays highly accurate predictions throughout the 1600+ FEC cycles evaluated. In cell C10, although a small discrepancy appears between 700 and 900 FEC, the model successfully corrects this behaviour further along the cycle range.

The metrics for Model 3 are reported in Table 5:

Table 5. SoH estimation errors for Model 3.

	Max. Error	**MAE**
Train	0.88%	0.12%
Validation	0.74%	0.12%
Test	1.32%	0.22%

A clear enhancement is observed compared to Model 2B. In the training phase, the maximum error decreased by 5.65%, and the MAE improved by 0.28%. Similar gains were recorded for the validation set (−5.43% max error, −0.31% MAE). The test phase also showed improvement, with a 4.77% reduction in max error and 0.34% in MAE.

4 Conclusions

This work has explored the development of several data-driven SoH estimation models based on artificial neural networks, using partial charging profiles. The aim was to design a robust estimator capable of working under partial data conditions, while progressively increasing model complexity to analyse its impact on accuracy and generalizability.

Model 1 represents the most basic architecture, relying exclusively on five input features extracted from the partial charging process. Its simplicity makes it suitable for both first-life and second-life battery applications, particularly because it does not require prior knowledge of the cell's history. However, this model fails to capture degradation trends, resulting in inaccurate SoH estimations and limited reliability.

To address this limitation, Model 2A introduces a time-based feature representing the elapsed time since the BoL. This addition enables the model to partially reconstruct degradation trajectories, improving estimation accuracy in most cases. However, the inclusion of the time variable compromises the model's applicability to second-life scenarios, where BoL data may be unavailable. Moreover, the model still exhibits sensitivity to the instantaneous temperature input, resulting in incorrect SoH estimations under thermal fluctuations.

Model 2B replaces the elapsed time variable with the number of FEC, a more intuitive and interpretable indicator of aging. This modification leads to further improvements, particularly in accurately capturing the degradation trend of more challenging cells, such as C10. Nonetheless, like Model 2A, Model 2B still presents an undesired correlation between the actual temperature and the predicted SoH values, leading to abrupt estimation peaks.

To overcome these limitations, Model 3 incorporates seven new features reflecting cumulative exposure to specific C-rate and temperature ranges. This historical perspective allows the model to account for long-term degradation stressors, mitigating the impact of transient operational conditions. As a result, Model 3 achieves the best performance across all evaluated phases—training, validation, and testing—with maximum error and MAE values of 1.32% and 0.22%, respectively. Furthermore, the SoH estimation curves produced by Model 3 exhibit significantly improved stability, eliminating the sharp fluctuations seen in previous models.

Despite the promising results, it must be emphasized that the models were trained under specific operating conditions, using controlled CC-CV charging protocols and cells with moderate degradation. Therefore, while Model 3 has demonstrated excellent accuracy within this context, its performance under realistic usage scenarios (e.g., variable current profiles, fast charging, or cells at the end of life) remains to be validated.

Acknowledgments

Funded by the Basque Government through the ELKARTEK Program: CICe2024, KK2024-00062: Deepening Knowledge for the Design and Development of New Electrolytes and Post-Lithium-Ion Battery Technologies.

References

[1] M. Li, J. Lu, Z. Chen, K. Amine, 30 Years of Lithium-Ion Batteries, Advanced Materials 30 (2018). https://doi.org/10.1002/adma.201800561.

[2] Y. Wang, J. Tian, Z. Sun, L. Wang, R. Xu, M. Li, Z. Chen, A comprehensive review of battery modeling and state estimation approaches for advanced battery management systems, Renewable and Sustainable Energy Reviews 131 (2020). https://doi.org/10.1016/j.rser.2020.110015.

[3] Y. Li, K. Liu, A.M. Foley, A. Zülke, M. Berecibar, E. Nanini-Maury, J. Van Mierlo, H.E. Hoster, Data-driven health estimation and lifetime prediction of lithium-ion batteries: A review, Renewable and Sustainable Energy Reviews 113 (2019). https://doi.org/10.1016/j.rser.2019.109254.

[4] C.R. Birkl, M.R. Roberts, E. McTurk, P.G. Bruce, D.A. Howey, Degradation diagnostics for lithium ion cells, J Power Sources 341 (2017) 373–386. https://doi.org/10.1016/J.JPOWSOUR.2016.12.011.

[5] M. Berecibar, I. Gandiaga, I. Villarreal, N. Omar, J. Van Mierlo, P. Van Den Bossche, Critical review of state of health estimation methods of Li-ion batteries for real applications, Renewable and Sustainable Energy Reviews 56 (2016) 572–587. https://doi.org/10.1016/j.rser.2015.11.042.

[6] M. Benavides, A. Arias, J.D. Cerdas, A. Perez, M. Orchard, Remaining Useful Life of Lithium-ion Batteries as a Function of the Joule Effect, in: 2020 IEEE International Autumn Meeting on Power, Electronics and Computing, ROPEC 2020, 2020. https://doi.org/10.1109/ROPEC50909.2020.9258726.

[7] L. Zhao, S. Song, P. Wang, C. Wang, J. Wang, M. Guo, A MLP-Mixer and mixture of expert model for remaining useful life prediction of lithium-ion batteries, Front Comput Sci 18 (2024). https://doi.org/10.1007/s11704-023-3277-4.

[8] S. Yang, C. Zhang, J. Jiang, W. Zhang, L. Zhang, Y. Wang, Review on state-of-health of lithium-ion batteries: Characterizations, estimations and applications, J Clean Prod 314 (2021) 128015.

https://doi.org/10.1016/J.JCLEPRO.2021.128015.
[9] J. Tian, R. Xiong, W. Shen, A review on state of health estimation for lithium ion batteries in photovoltaic systems, ETransportation 2 (2019). https://doi.org/10.1016/J.ETRAN.2019.100028.
[10] L. Ungurean, G. Cârstoiu, M. V. Micea, V. Groza, Battery state of health estimation: a structured review of models, methods and commercial devices, Int J Energy Res 41 (2017) 151–181. https://doi.org/10.1002/er.3598.
[11] M.S.H. Lipu, M.A. Hannan, A. Hussain, M.M. Hoque, P.J. Ker, M.H.M. Saad, A. Ayob, A review of state of health and remaining useful life estimation methods for lithium-ion battery in electric vehicles: Challenges and recommendations, J Clean Prod 205 (2018). https://doi.org/10.1016/j.jclepro.2018.09.065.
[12] C. Vidal, P. Malysz, P. Kollmeyer, A. Emadi, Machine Learning Applied to Electrified Vehicle Battery State of Charge and State of Health Estimation: State-of-the-Art, IEEE Access 8 (2020) 52796–52814. https://doi.org/10.1109/ACCESS.2020.2980961.
[13] Y. Feng, C. Xue, Q.-L. Han, F. Han, J. Du, Robust Estimation for State-of-Charge and State-of-Health of Lithium-Ion Batteries Using Integral-Type Terminal Sliding-Mode Observers, IEEE Transactions on Industrial Electronics 67 (2020). https://doi.org/10.1109/TIE.2019.2916389.
[14] H. Pan, Z. Lü, H. Wang, H. Wei, L. Chen, Novel battery state-of-health online estimation method using multiple health indicators and an extreme learning machine, Energy 160 (2018) 466–477. https://doi.org/10.1016/j.energy.2018.06.220.
[15] K.Q. Zhou, Y. Qin, C. Yuen, Transfer-Learning-Based State-of-Health Estimation for Lithium-Ion Battery With Cycle Synchronization, IEEE/ASME Transactions on Mechatronics (2022). https://doi.org/10.1109/TMECH.2022.3201010.
[16] Y. Li, H. Sheng, Y. Cheng, D.I. Stroe, R. Teodorescu, State-of-health estimation of lithium-ion batteries based on semi-supervised transfer component analysis, Appl Energy 277 (2020) 115504. https://doi.org/10.1016/j.apenergy.2020.115504.
[17] K. Deb, S. Agrawal, A. Pratap, T. Meyarivan, A Fast Elitist Non-dominated Sorting Genetic Algorithm for Multi-objective Optimization: NSGA-II, Lecture Notes in Computer Science (Including Subseries Lecture Notes in Artificial Intelligence and Lecture Notes in Bioinformatics) 1917 (2000) 849–858. https://doi.org/10.1007/3-540-45356-3_83.
[18] Z. Chen, M. Sun, X. Shu, J. Shen, R. Xiao, On-board state of health estimation for lithium-ion batteries based on random forest, in: Proceedings of the IEEE International Conference on Industrial Technology, 2018. https://doi.org/10.1109/ICIT.2018.8352448.
[19] L. Song, K. Zhang, T. Liang, X. Han, Y. Zhang, Intelligent state of health estimation for lithium-ion battery pack based on big data analysis, J Energy Storage 32 (2020). https://doi.org/10.1016/j.est.2020.101836.
[20] H. Zhang, L. Zhang, Y. Jiang, Overfitting and Underfitting Analysis for Deep Learning Based End-to-end Communication Systems, 2019 11th International Conference on Wireless Communications and Signal Processing, WCSP 2019 (2019). https://doi.org/10.1109/WCSP.2019.8927876.

Presenter Biography

Markel Azkue received his M.Sc in Industrial Engineering from the University of Mondragon in 2020. He joined the Energy Storage and Management unit of Ikerlan Technology Research Centre (BRTA), Spain, in 2016. He obtained his Ph.D. in Applied Engineering with international mention in 2023, focused on Battery SoC and SoH estimation algorithms using AI. He is currently working as a researcher on projects related to lithium-ion batteries. His research interests include machine learning algorithms applied to electrochemical energy storage systems state estimators.